Geochemistry 85 (2025) 126244

Contents lists available at ScienceDirect

Geochemistry

journal homepage: www.elsevier.com/locate/chemer

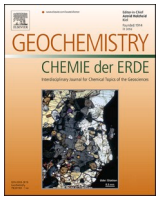

Sideritization and silification of unconformity-related hydrothermal baryte veins near Grünau, south Namibia

Benjamin F. Walter [a,*], Manuel Scharrer [b], R. Johannes Giebel [c,d], Aratz Beranoaguirre [e], Jorge C.L. Arthuzzi [f,g], Lorenz Kemmler [c,d], Andreja Ladisic [a], Saskia Dück [c,d], Michael Marks [a], Gregor Markl [a]

[a] Eberhard Karls University Tübingen, Department of Petrology and Mineral Resources, Schnarrenbergstraße 94-96, 72074 Tübingen, Germany
[b] School of Molecular Sciences and Center for Materials of the Universe, Arizona State University, Tempe, AZ 85287, United States
[c] Technische Universität Berlin, Department of Applied Geochemistry, Ernst-Reuter-Platz 1, 10587 Berlin, Germany
[d] University of the Free State, Department of Geology, 250 Nelson-Mandela-Drive, 9300 Bloemfontein, South Africa
[e] Frankfurt Isotope and Element Research Center (FIERCE), Goethe-Universität Frankfurt, Frankfurt, Germany
[f] Karlsruhe Institute of Technology (KIT), Chair of Geochemistry and Economic Geology, Adenauerring 20b, 76131 Karlsruhe, Germany
[g] Laboratory of Environmental and Raw Material Analyses (LERA), Adenauerring 20b, 76131 Karlsruhe, Germany

ARTICLE INFO

Handling Editor: Martina Zucchi

Keywords:
Fluid mixing
Pangea breakup
Fluid inclusions
Thermodynamic modelling
TitaniQ

ABSTRACT

The development of economic mineralization within unconformity related hydrothermal vein type deposits is a topic of basic (but also economic) significance. In particular late-stage processes like pseudo- or perimorphic replacements can significantly influence the mineralogy and hence processability of ore deposits. This study aims to shed light on such late stage processes leading to the mineralogical modification of primary hydrothermal veins by pseudomorphous and perimorphous replacements of quartz after hydrothermal gangue minerals like carbonates, baryte and fluorite; whereas the genesis of pseudomorphic replacements of baryte by siderite and a contemporaneous perimorphic overgrowth of quartz has not been studied in detail so far. To study this process, hydrothermal veins of the south Namibian hydrothermal vein type district, which are related to the breakup of Pangea are chosen as natural laboratories.

Fluid inclusion data together with a detailed petrography of the paragenetic sequence and fluid inclusion assemblages reveal a temperature drop from early quartz I at ~170 °C down to ~80 °C in quartz III at almost constant salinities of 23.1 to 24.5 wt% ($NaCl+CaCl_2$). The chemistry of the observed fluid inclusion assemblages is in accordance with previous microthermometry studies carried out in the same hydrothermal vein type district indicating an identical provenance of the fluids recognized in the other deposits (e.g., Aukam and Garub). Hence it is likely that a high salinity basement brine of cryogenic origin has been mixed with a Nama Group limestone derived fluid to form the primary mineralization. Mixing of two chemically-contrasted fluids is also depicted by the trace elements studied in the youngest quartz generation whereas the application of the TitaniQ thermometer provide evidence for a temperature of about 320 °C in the deep-seated reservoir which became afterwards mixed with Nama Group limestone derived fluids. Thermodynamic modelling based on the gathered fluid data and data from analogue studies, provide evidence that siderite pseudomorphs after baryte form under reducing conditions, under which sulfate is reduced and the dissolution of baryte promotes siderite and pyrite precipitation. Hence, the present study contributes to the still weakly developed understanding how post-precipitation processes influences the mineralogy of hydrothermal veins.

1. Introduction

Baryte, fluorite, quartz, carbonates and anhydrite/gypsum are common gangue minerals in hydrothermal veins. Pseudomorphous and perimorphous textures of quartz after those gangue minerals are common worldwide (Baier et al., 1961; Baumann et al., 2000; Leach et al., 2004; Burisch et al., 2017) and typically named as “bladed quartz”. In contrast to pseudomorphism, where the primary phase is replaced

* Corresponding author.
E-mail address: b.walter@uni-tuebingen.de (B.F. Walter).

https://doi.org/10.1016/j.chemer.2024.126244
Received 18 July 2024; Received in revised form 10 December 2024; Accepted 23 December 2024
Available online 27 December 2024

during dissolution-precipitation processes by a secondary phase, perimorphism is characterized by dissolution of the primary phase that is overgrown by a resistant secondary phase (no replacement of the primary phase). This often leads to negative crystals shapes (e.g. perimorphous cubes of quartz after fluorite). As it is known from numerous hydrothermal mining districts, the existence of bladed quartz may indicate a significant reduction of metal and non-metal mineral resources in numerous deposits and, therefore, represents an important exploration indicator (e.g. veins in the Schwarzwald mining district; Burisch et al., 2017; Walter et al., 2019). The processing of silicified fluorite and baryte ores can be complicated and expensive, and, therefore, reduces the value of the deposit. Examples (silification of primary gangue minerals and pseudomorphous bladed quartz) are known from the well-studied Schwarzwald mining district (Burisch et al., 2017), from hydrothermal veins in the Odin Forest, Germany (Baier et al., 1961), the Ore Mountains, Germany (Baumann et al., 2000), Queensland, Australia (Dong et al., 1995), the De Lamar district, USA (Lindgren, 1899), Elk County, USA (Schrader, 1912), the Martha lode, New Zealand (Morgan, 1925) and the Brooks Range, Alaska, USA (Leach et al., 2004), etc.

However, although the processes inducing pseudomorphism and perimorphism has been known for >150 years (Sandberger, 1891) they are surprisingly weakly studied. As previously stated by Burisch et al. (2017) only few authors interpreted the silification in hydrothermal system and concluded it as a "quartz root" of hydrothermal baryte-fluorite vein deposits (Bliedtner and Martin, 1986; Liessmann, 2010). Burisch et al. (2017) demonstrated that textural observations clearly identify such a silification as a late-stage phenomenon (replacement process), which is not contemptuously with the main phase of the hydrothermal mineralization. This contribution emphasizes hydrothermal baryte-siderite-quartz veins in southern Namibia, where a perimorphic replacement of quartz after baryte and a pseudomorphic replacement of siderite after baryte is observed. The aim is a comprehensive study of textures and a thermodynamic model for the coupled pseudomorphic and perimorphic processes. Hence, this study will present fluid inclusion data (fluid chemistry and homogenization temperatures) from pre- and post-replacement quartz to shed light on the genesis of the hydrothermal veins and the related replacement processes. To model the replacement processes in detail fluid inclusion data were used as input parameters for the thermodynamic modelling approach. Such a coupled process has never been addressed by a modern fluid inclusion study combined with LA-ICPMS trace element data of quartz and thermodynamic modelling.

1.1. Unconformity related hydrothermal veins in South Namibia

The genesis of the hydrothermal system in southern Namibia is weakly studied, with only single occurrences being investigated so far (for details on the geology and formation models of the Aukam and Garub fluorite-baryte-quartz deposits, the reader is kindly referred to Walter et al., 2024, Walter et al., 2023). In contrast, small scale mining on hydrothermal fluorite ± baryte ± quartz ± carbonate veins hosting Cu-Pb-Zn-Ag mineralization in southern Namibia was widespread, in particular between 1900 and 1950 with the Garub and Aukam fluorite-baryte-quartz deposits being of local importance (Walter et al., 2023, 2024). Most recently, Walter et al. (2023, 2024) provided evidence for fluid mixing between two high salinity brines being the major process generating hydrothermal veins in this region. As shown in previous contributions, a deep-seated high salinity brine of elevated temperatures (>250 °C) is mixed with an almost equally saline, Nama Group limestone derived fluid. Most of the known hydrothermal fluorite-baryte-quartz veins show thicknesses of centimetre to meter scale and can be followed for up to hundreds of meters (e.g. Aukam; Walter et al., 2023; Garub; Walter et al., 2023; Jerusalem deposit, Ausenkehr deposit, Bokkiesbank Ost 79, Blyderverwacht 72, Altdorn 3, AiAis Mine/Kanabeam 331, Lübeck 2, Kwaggasnek 349; Weltevrede 302; Mickberg 474; Hoal, 1990) are hosted by metamorphic rocks of the Namaqua-Natal-Metamorphic-Complex less than a few hundred meters below the Nama Group unconformity (Fig. 1A, B, C, D, 2C; Walter et al. 2023a, 2023b). Most of the hydrothermal veins follow structures associated with the opening of the South Atlantic Ocean (Corner, 2000; Walter et al. 2023a, 2023b). Only hydrothermal veins at Elandsdraai 71 crosscut the basis of the sedimentary Nama Group.

1.2. The hydrothermal veins and gathered sample material

The analysed vein at Weltevrede farm (Fig. 1 and 2A-E) is about 40 cm thick and can be traced for about 100 m at surface (for more information on the regional geological frame work please see Corner, 2000; Walter et al. 2023a, 2023b). At Mickberg farm, a further quartz vein shows a thickness of about 30 cm. Both veins positively weather out of the gneiss country rock (Namaqua-Natal-Metamorphic-Complex, Fig. 2) and transect the Weltevrede and Mickberg carbonatites (~550 Ma). The primary/original veins consisted of baryte, which is overgrown by quartz I (Fig. 3A-C). If present, baryte only occur as relicts now. Sulfides (mainly chalcopyrite and pyrite, very minor galena, sphalerite) are always hosted by quartz I. Pseudomorphic replacements of siderite after baryte is common. Up to centimetre large pyrite crystals are directly associated with the siderite pseudomorphs. The siderite formed at the same time or shortly before the perimorphic replacement of baryte by quartz II. Perimorphic replacement of quartz II after baryte accounts together or shortly after siderite formation. The perimorphic quartz II again is overgrown by a late-stage quartz III, which is characterized by euhedral quartz crystals up to 20 cm in length (Fig. 3D, E). Due to intense silification, the veins were never targeted for exploration and mining.

2. Methods

2.1. Fluid inclusion and crush leach analyses

Cathodoluminescence microscopy of quartz was applied to yield "hidden" textures, (e.g. multiple mineral growth zones, alteration, formation and healing of fractures) to correctly determine the fluid petrography and timing of fluid inclusion assemblages (e.g. Kolchugin et al., 2016, 2020; Kreissl et al., 2018; Epp et al., 2019; Mueller et al., 2020, 2022a, 2022b; Müller et al., 2024). A 'hot cathode' CL microscope (type HC1-LM) at the University of Tübingen was used with an electron beam acceleration voltage of ~14 kV and a beam current density of ~9 μAmm−2 on the sample's surface.

Microthermometric analysis was applied by using a Linkam THMS600 heating-freezing stage at the Karlsruhe Institute of Technology (KIT) hosted Laboratory for Environmental and Raw Material Analysis (LERA). For machine calibration synthetic, quartz-hosted H_2O, H_2O-NaCl and H_2O-CO_2 fluid inclusion reference materials (SynFlinc Standard collection) were used and measured on a daily basis. The samples were cut perpendicular to the wall of the hydrothermal vein. Five, representative doubly-polished thick sections (300–400 μm) were prepared and after optical microscopy and petrography sliced into chips. The fluid inclusion assemblages and petrography of each fluid inclusion was documented via transmitted light microscopy following the approach of Goldstein and Reynolds (1994). The documented fluid inclusion assemblages (FIA) were brought into a genetic relationship and classified as primary inclusions (p) hosted by crystal growth zones, pseudo-secondary (ps), secondary (s), isolated inclusions (iso) or clusters (c) with no genetic relationship and no geometrical orientation to growth zones or fractures (classification after Walter et al., 2015). For each analysis, triplet measurements were applied to obtain data of the final melting temperature of ice ($T_{m,ice}$) and hydrohalite ($T_{m,hh}$) and (2) the homogenization temperature (T_h). For interpretation of the data, only fluid inclusion data for which repeated analyses show a deviation of <0.1 °C for $T_{m,ice}$, $T_{m,hh}$, $T_{t,CO2}$, $T_{m,clath}$ and < 1 °C for T_h are used. The interpretation excludes fluid inclusions showing evidence for metastable

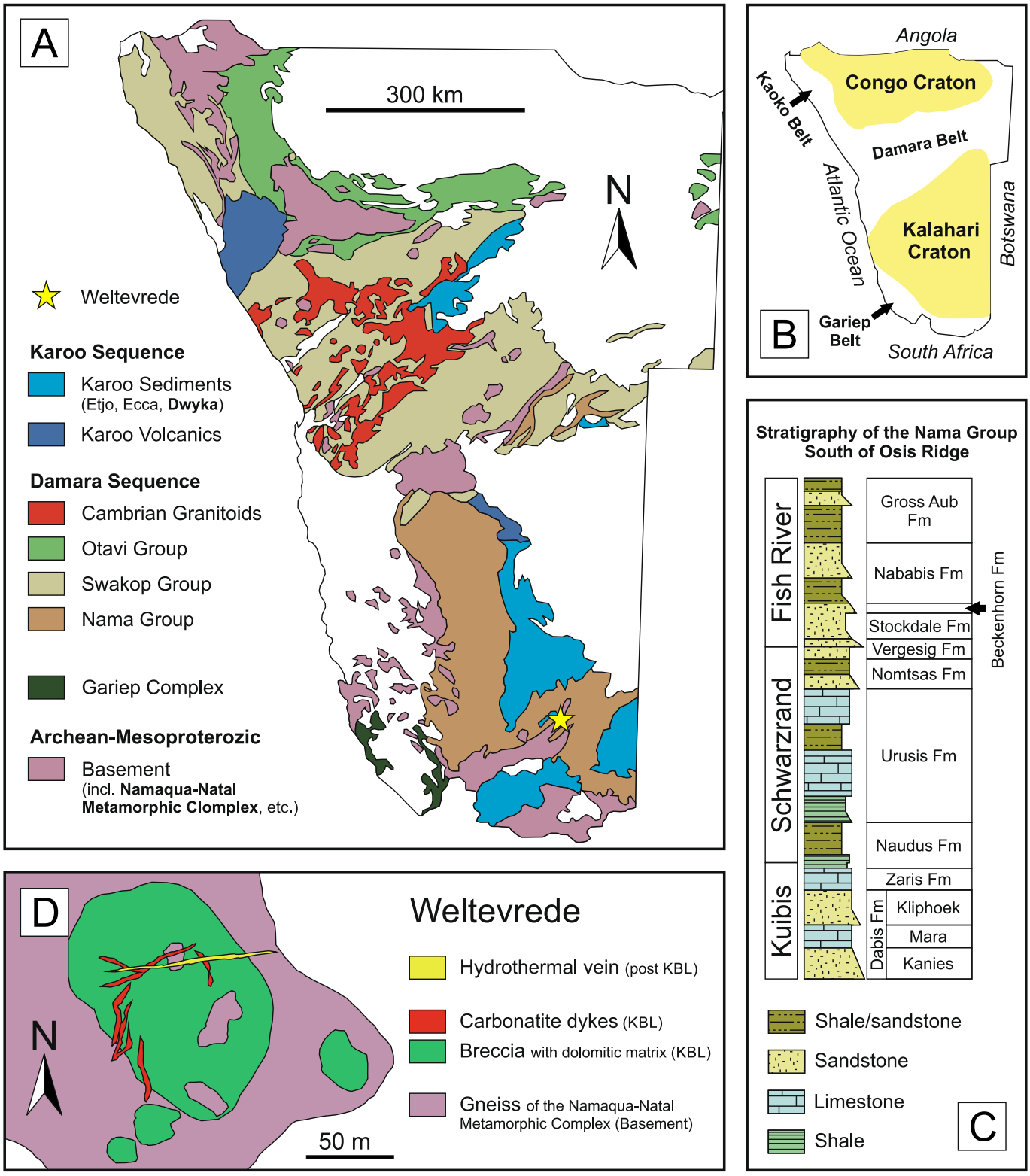

Fig. 1. (A) Simplified geological map of Namibia (modified after Walter et al., 2022). (B) Geological map of the Weltevrede complex with the transecting hydrothermal vein.

absence of hydrohalite, which were identified by applying the Gibb's law in the system-related phase diagram NaCl-H_2O-$CaCl_2$ (e.g. Steele-MacInnis et al., 2011). Pressure correction was applied by using the HOKIEFLINCS_H2O-NACL program of Steele-MacInnis et al. (2012) with estimated 1000 m Nama Group overburden at time of hydrothermal vein formation (Grotzinger et al., 2005).

2.2. LA-ICPMS Trace elements in quartz

In-situ trace element compositions of quartz were obtained by laser ablation inductively coupled plasma mass spectrometry (LA-ICP-MS) using a Teledyne Analyte Excite+ ArF (193 nm) excimer laser ablation system coupled to a Thermo-Scientific Element XR sector field mass

Fig. 2. (A) Mineralized sample of the hydrothermal vein at Weltevrede. (B) Large, positively weathered out blocks of vein material emerge from the gneiss country rocks. (C) Namaqua-Natal-Metamorphic Complex-Nama Group unconformity about 200 m above outcrop. (D) Outcropping hydrothermal vein at Weltevrede. (E) Large quartz geods (occasionally formed in the vein at Weltevrede).

spectrometer at LERA, KIT. For analysis, a laser spot size of 65 μm, a pulse rate of 10 Hz and a fluence of 7.0 J/cm2 were used. Samples were ablated in a He atmosphere (0.5 l/min) to which 8–11 ml/min N_2 and ~ 0.85 l/min Ar were added directly after the ablation cell. The ICPMS was tuned for maximum sensitivity while keeping the oxide formation (UO/U < 0.1 %) and element fractionation low (i.e., Th/U = ~1). All data were acquired and reduced in blocks of 30 unknowns bracketed by SRMNIST-612 glass reference material (Pearce et al., 1997; Jochum et al., 2011). Data were processed using the Iolite data reduction software (Paton et al., 2011). All signals were normalized to 29Si as an internal standard using 100 wt% SiO_2 for data reduction of quartz analyses. To monitor accuracy, SRMNIST-614 glass was analysed as an unknown and yielded trace element contents of Be = 0.82 ± 0.5 ppm (2σ), Ti = 3.2 ± 0.1 ppm (2σ), Co 0.74 ± 0.03 ppm (2σ), Ni = 1.16 ± 0.07 ppm (2σ), Zn = 2.8 ± 0.4 ppm (2σ), Ge = 1.03 ± 0.09 ppm (2σ), Rb = 0.89 ± 0.04 ppm (2σ), Nb = 0.89 ± 0.03 ppm (2σ), Mo = 0.81 ± 0.05 ppm (2σ), In = 0.86 ± 0.06 ppm (2σ), Sb = 0.77 ± 0.04 ppm (2σ), W = 0.78 ± 0.05 ppm (2σ), Au = 0.55 ± 0.04 ppm (2σ), Pb = 2.6 ± 0.3 ppm (2σ) and Bi = 0.62 ± 0.05 ppm (2σ), which agree with published values of Jochum et al. (2011).

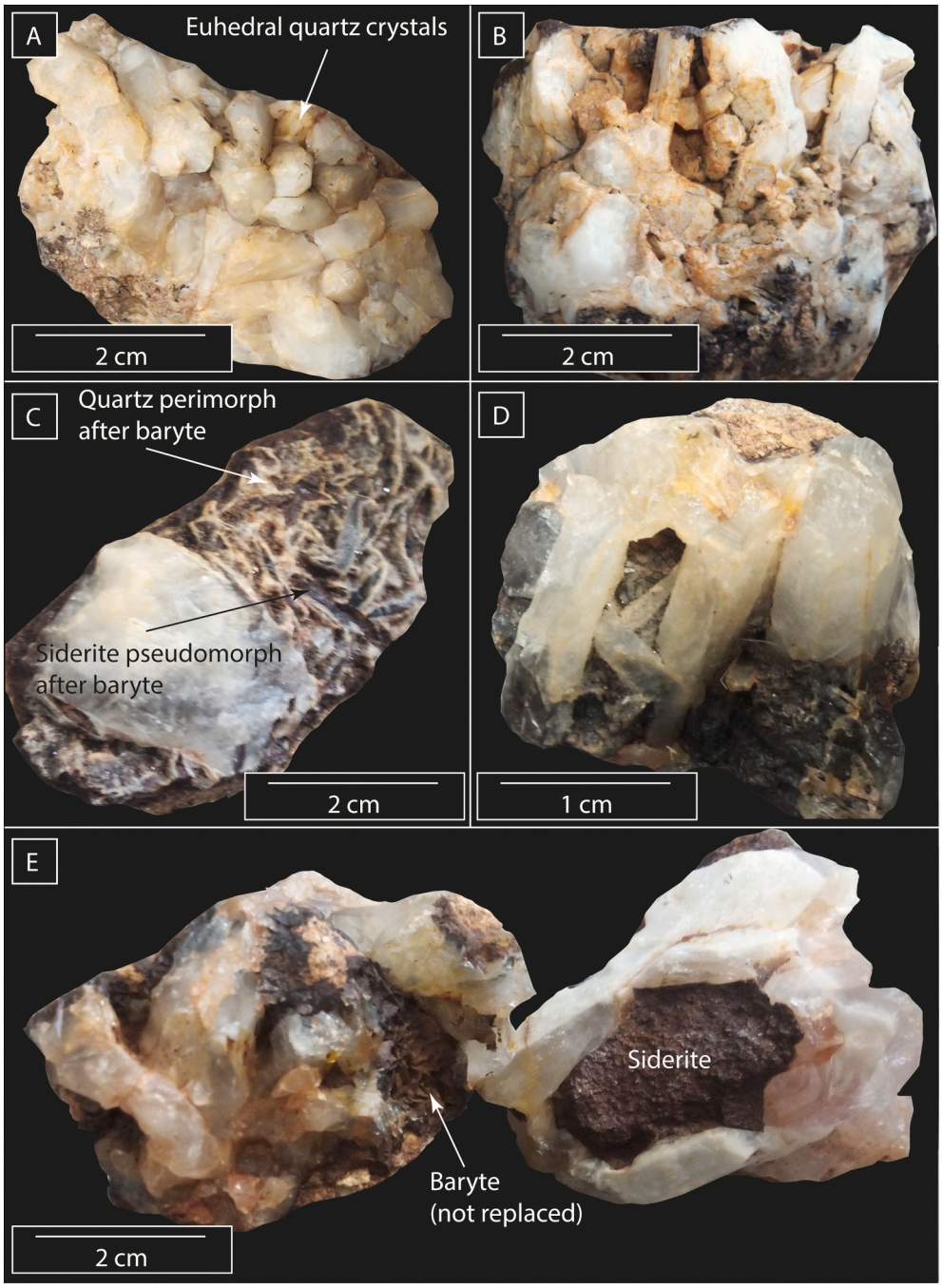

Fig. 3. (A) Euhedral Qtz III crystals overgrow baryte that is replaced by siderite (replacement visible in 3c). (B) Siderite I is overgrown by anhedral Qtz II and euhedral Qtz III. (C) Qtz II forms perimorphic textures after baryte, whereas Sid I form pseudomorphic replacements after baryte. (D) Euhedral Qtz III with growth zones. (E) Original euhedral baryte, which is not replaced by Qtz II. Siderite I occur as either euhedral rhombs or as peudomorphic replacements after baryte and is today partly replaced hematite.

2.3. *Thermodynamic modelling*

Thermodynamic fluid modelling was achieved by the use of the 15th Dec. 2020 Thermoddem version thermodynamic database (Blanc, 2017; Blanc et al., 2012) and the thermodynamic modelling software PHREEQC version 3.7.3 (Parkhurst, 1995; Parkhurst and Appelo, 1999) and PHREEPLOT version 1.0 (Kinniburgh and Cooper, 2011).

Unfortunately, exact fluid compositions remain unknown due to a lack in primary fluid inclusions of the siderite that can be analysed by LA-ICP-MS. As realistic input conditions, compositional ranges are chosen based on abundant compositional studies of hydrothermal veins in the region and crush leach (this study, Walter et al., 2023, Walter et al., 2023). Fluid compositions were varied to study the impact of composition on mineral stability. Based on the known fluid compositions, a 25 wt% NaCl saline H_2O fluid is chosen as the basis and minor/trace elements are varied and presented accordingly at each modelled diagram.

3. Results

3.1. Petrography and fluid petrography

Assignment and labelling of fluid inclusion generations were done according to the nomenclature reflected in Fig. 4. Quartz I exclusively contain isolated fluid inclusions (isoQtz1–1) that are neither crystallographically oriented nor aligned along visible fractures. The inclusion sizes vary between <5 μm and up to 50 μm. The inclusions of isoQtz1–1 are typically rounded and often show evidence for post-entrapment modifications like "necking down" and decrepitation. The fluid inclusions were carefully selected for measurements and only inclusions for which post-entrapment modifications can be ruled out were studied. Quartz I typically contain small (10–20 μm) nests of chalcopyrite. In baryte I, all fluid inclusions got damaged during preparation as common for baryte. The pseudomorphic replacement of baryte by siderite I is fluid inclusion free. Only isolated fluid inclusions (5–50 μm in size) are rarely observed in euhedral siderite I crystals that were grown simultaneously to the siderite-baryte replacement. In contrast, the perimorphous quartz II after siderite has only clusters of fluid inclusions (cQtz2–1) and pseudo-secondary fluid inclusions (psQtz1–1). For both inclusion sizes, between 5 and 40 μm are common. The inclusions are typically rounded or elongated. In paragenesis with quartz II large (up to 5 cm) pyrite crystals can be observed that are overgrown by quartz III. The euhedral quartz III growing on top of quartz II contains primary fluid inclusions in two assemblages (pQtz3–1, pQtz3–2). For both assemblages the inclusions are tiny (<5–10 μm) and angular (c.f. Fig. 6A). The entire system is finally overgrown by calcite that lacks any fluid inclusions (Fig. 5).

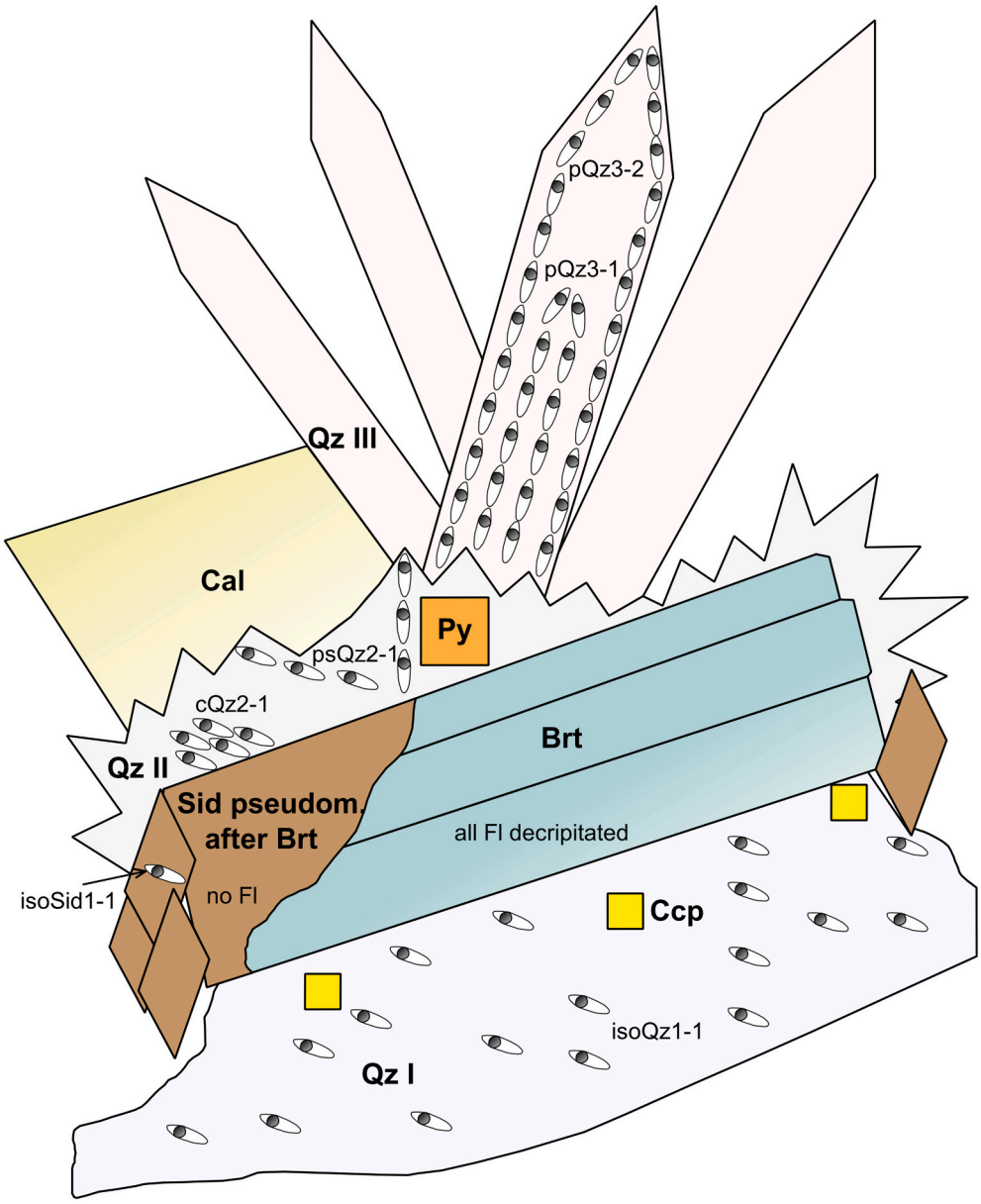

Fig. 4. Sketch of the observed paragenesis and related fluid inclusion assemblages. Quartz I hosts isolated fluid inclusions (isoQtz1–1) and nests of chalcopyrite (Ccp). Baryte (Brt) is completely free of fluid inclusions as thus were damaged during preparation. The pseudomorphous siderite (Sid) after baryte are also fluid inclusions free, while the simultaneously formed euhedral siderites show isolated fluid inclusions (isoSid1–1). Quartz II contains only clusters of fluid inclusions (cQz2–1) as well as pseudo-secondary fluid inclusions (psQz2–1) with occasionally occuring pyrite crystals (Py). The euhedral quartz III has primary fluid inclusions. This system is overgrown by fluid inclusion free calcite.

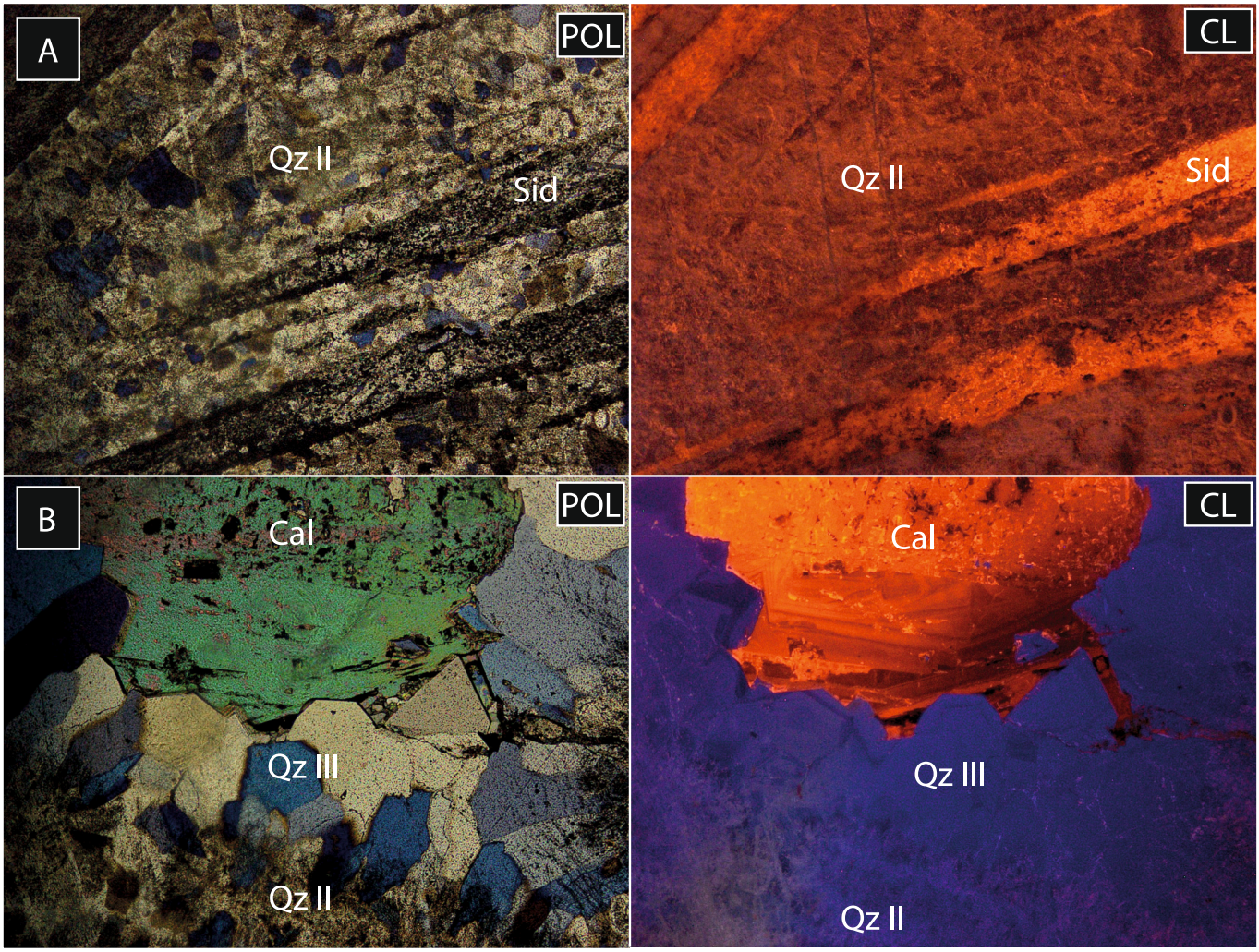

Fig. 5. (A, B) Microtextures of bladed quartz in transmitted light (left side) and under cathodoluminescence (right side). A) Baryte plates are replaced by siderite, which is again overgrown by perimorphic quartz. B) The figure illustrates the transition between quartz II (forming a perimorphic replacement) and quartz III (euhedral crystals overgrowing quartz II). The calcite shows complex zoning pattern, typical for low temperature hydrothermal systems.

3.2. Fluid systematics

In course of this study, QtzI-III and SidI provided appropriate fluid data which are summed up in Table 1 and Fig. 6. The complete data set is provided in the Electronic Supplement ES1. The majority of fluid inclusions were relatively small (typically below 20 μm) and angularly shaped. Only exceptionally larger fluid inclusions can be observed (Fig. 6A). Numerous fluid inclusions show evidence for post-entrapment modifications and therefore the data was carefully considered to exclude all measurements for which post-entrapment modifications cannot strictly be ruled out. As shown in Table 1, the data within a fluid inclusion assemblage is homogenous, which is a further criterion for the data quality.

3.3. Trace elements in quartz

The trace elements in quartz III were measured along a profile from early to late growth zones (ES3). In general, the trace element content is very low for most elements (Fig. 7). Only Na, Al, Ca reach elevated concentrations up to 1545 ppm, 1630 ppm and 170 ppm, respectively. The Li distribution behaves similar to Al but shows significant lower concentrations of ~10 to <100 ppm. All other trace elements are usually below 10 ppm. Trace element pattern exhibit an unsystematic behaviour for most of the quartz-growth-profile with a significant drop at the end of the profile. Thereby Na and Ca decrease below the detection limit, while Al depletes by two log unit and Li by one log unit of concentration. Most of the trace elements also fall below detection limits at the end of the profile.

Table 1
Summary of the observed fluid parameters.

Mineral	Assemblage (No of FI)	$T_{m,ice}$ (°C)	$T_{m,hh}$ (°C)	T_h (°C)	Salinity ($NaCl+CaCl_2$)	Mole Ca/(Na + Ca)
Qtz I	isoQtz1–1 ($n = 8$)	−22.7 to −25.8	−25.4 to −26.8	140–162	23.1–24.4	0.30–0.39
Sid I	isoSid1–1 (n = 10)	−22.8 to −23.5	−24.3 to −26.0	104–120	23.2–23.8	0.23–0.34
Qtz II	cQtz2–1 ($n = 10$)	−22.8 to −24.5	−25.0 to −25.8	90–104	23.3–24.3	0.28–0.32
Qtz II	psQtz2–1 ($n = 12$)	−22.1 to −23.8	−25.1 to −26.3	73–84	22.7–23.7	0.28–0.36
Qtz III	pQtz3–1 (n = 10)	−22.4 to − 24.2	−25.3 to −26.7	58–66	22.9–23.9	0.30–0.38
Qtz III	pQtz3–2 (n = 12)	−22.4 to − 23.5	−25.8 to −26.8	49–62	22.8–23.3	0.32–0.39

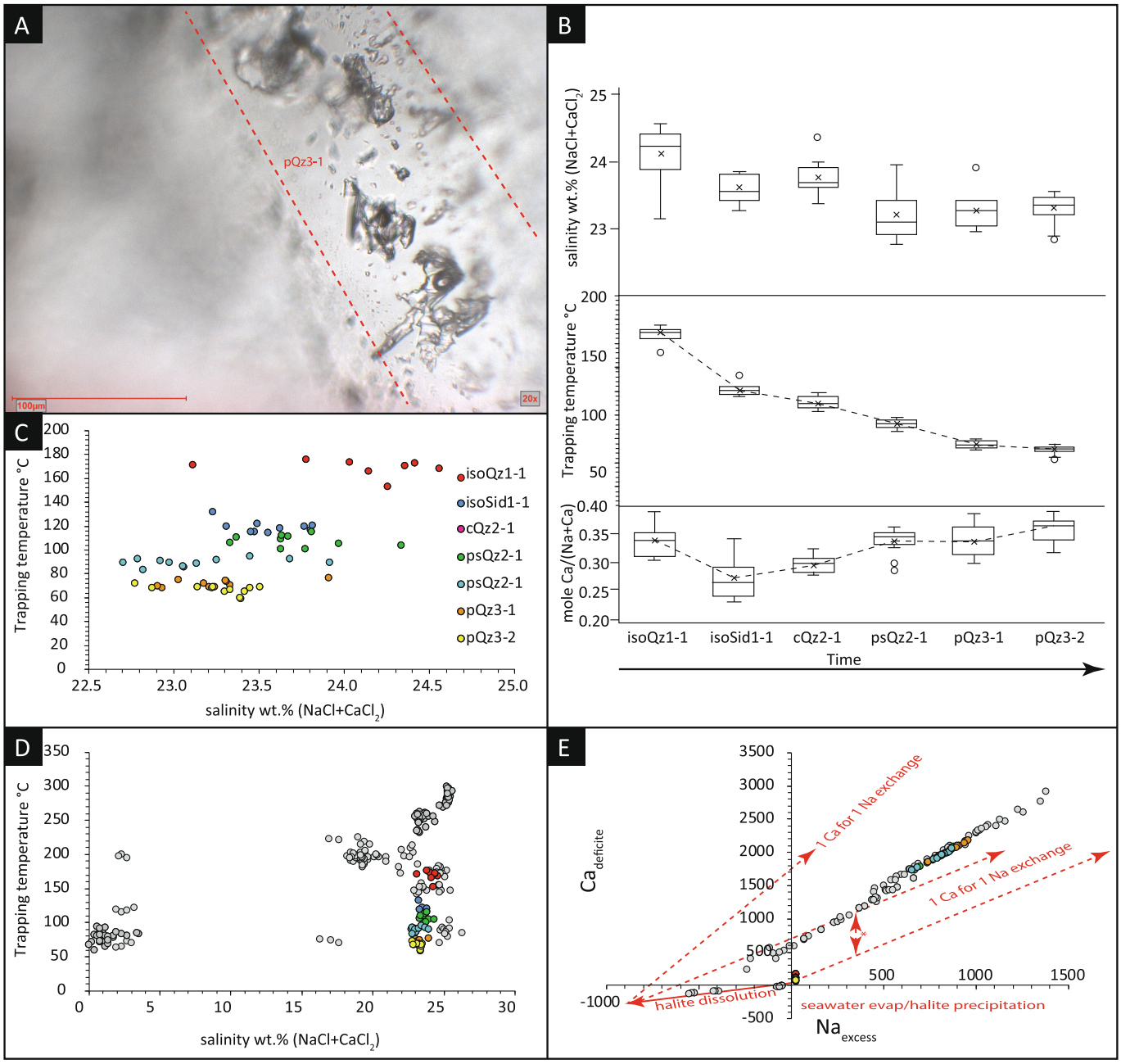

Fig. 6. (A) Growth zone with primary fluid inclusions. (B) Evolution of salinity, trapping temperatures and Ca/(Na + Ca) mole ratios with time. (C) Trapping temperatures versus salinity. Note. Data indicates a trend from higher salinity and hotter temperatures towards slightly lower salinities at lower temperatures. (D) Comparison of Weltevrede fluids and fluids analysed in the Aukam valley and the Garub fluorite mine (grey data points; data from Walter et al., 2023, c). (E) Na_{excess}-$Ca_{deficite}$ diagram after Davisson and Criss (1996). Note: The data show a complex history of halite dissolution and basement water rock interaction. Data from Aukam valley and the Garub fluorite mine (grey data points) are taken from Walter et al. (2023, 2024).

Titanium concentrations between 0.02 and 0.86 ppm lead to temperatures between 236 °C and 381 °C by application of the TitaniQ thermometer (Wark and Watson, 2006) with a Gaussian distribution and a mean at 320 °C.

4. Discussion

4.1. Timing and formation process of primary hydrothermal veins at Weltevrede and Mickberg

The hydrothermal quartz veins of Weltevrede and Mickberg both crosscut Namaqua-Natal-Metamorphic-Complex gneisses (1.1 Ga; Macey et al., 2022) and Kuboos-Bremen line related carbonatite intrusions (~ 550 Ma; Verwoerd, 1967; Reid et al., 1990). Based on crosscutting relationships and studies on the structures hosting the hydrothermal veins in south Namibia, a younger Mesozoic age is most likely and their genesis is potentially related (as a far field consequence) to the opening of the Atlantic Ocean (Burisch et al., 2022; Walter et al., 2023). Unfortunately, it is not feasible to constrain an absolute age due to the lack of datable minerals in the hydrothermal veins. To understand the observed replacement textures the processes generating the primary vein are discussed and afterwards discriminated from the late stage processes generating the replacements.

To understand the formation processes of the hydrothermal veins at Weltevrede and Mickberg it is important to compare these veins with other hydrothermal veins in a regional scale. An evaluation indicates

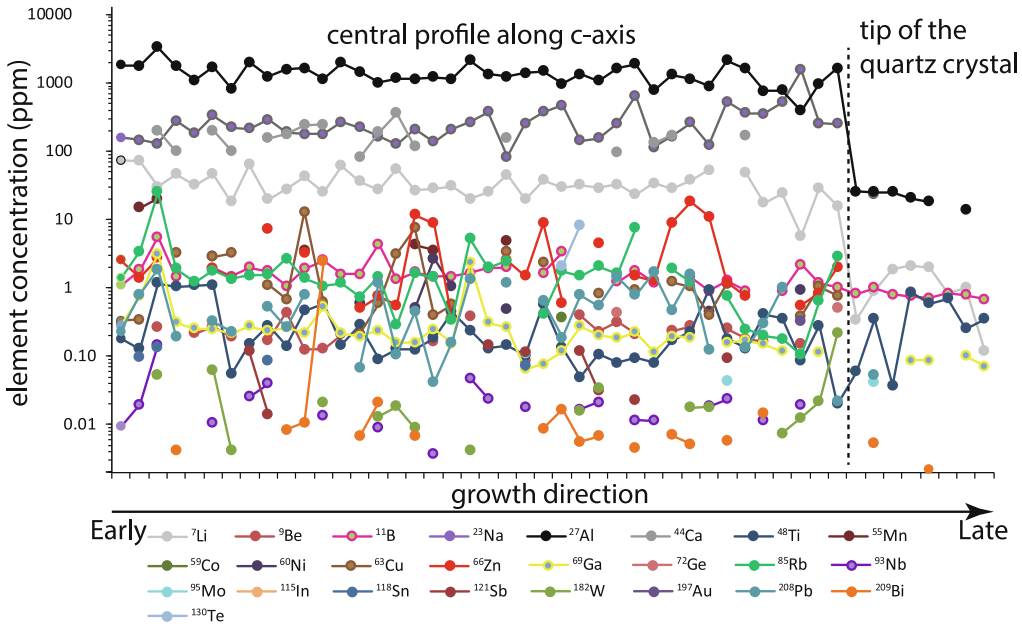

Fig. 7. Trace element pattern of quartz. The x-axis reflects the cross-section through a quartz crystal from left (early) to right (late).

that fluorite veins in the Aukam valley and at the Garub farm in southern Namibia (Walter et al., 2023, Walter et al., 2024) have very similar high salinity brine compositions (Fig. 6D and E) and a very similar structural framework hosting the veins. For both occurrences a brine mixing that caused the precipitation of fluorite, baryte, quartz and carbonates is proclaimed (Walter et al. 2023a, 2023b). Due to the absence of evaporates in the Nama Group sedimentary rock overburden, timing and origin of brine generation is likely related to cryogenic processes at the base of the Dwyka ice shield that covers Namibia in Permian times (for more details on the cryogenic brines, the reader is referred to the discussion in Walter et al., 2024), while the opening of fluid pathways is likely related to the break-up of Pangea in Jurassic-Cretaceous times (Walter et al., 2023). Since the geological setting and structural framework is equal for the south Namibian occurrences (for more information on the geology and precipitation process see Walter et al., 2023, Walter et al., 2023), and fluid chemistry of the hydrothermal veins of this contribution are very similar to the ones studied at Aukam valley and Garub farm, a Jurassic-Cretaceous age is also very likely. Therefore, the hydrothermal baryte veins at Weltevrede and Mickberg are likely a further type of hydrothermal veins formed from the widespread hydrothermal event, generating the fluorite veins at Aukam valley and Garub farm (Walter et al., 2023, 2024). Most likely this event caused further unstudied hydrothermal veins at e.g., the Jerusalem deposit, Ausenkehr deposit, Elandsdraai 71; Bokkiesbank Ost 79, Blyderverwacht 72, Altdorn 3, Ai-Ais Mine/Kanabeam 331, Lübeck 2 and Kwaggasnek 349 (Hoal, 1990). The missing fluorite formation in Weltevrede and Mickberg might be caused by the multivariant mineral formation deviations of the hydrothermal system (e.g. variation in fluorine content of the source, fluorine complexation, stabilities of hydrothermal calcium precipitates and dominance of HCO_3^-, etc).

Trace element pattern, generated by LA-ICPMS analyses show an unsystematic scattering between higher and lower trace element contents in the growth direction of the quartz crystals. This unsystematic scattering points to a formation of Qtz I-III by fluid mixing of the two endmembers already identified in Walter et al. (2023 2024) as analytical artefacts can be excluded. Additional the precipitation process is combined with a strong fluid cooling component. Endmember 1 is likely a cryogenic brine that interacted with the metamorphic basement (halite saturated brine, see discussion in Walter et al., 2023, 2024), whereas fluid endmember 2 is suggested to have interacted with Nama Group limestone (halite dissolution brine, see Na_{excess}-$Ca_{deficite}$ diagram in Fig. 6F). To explain the presence of sulfides in baryte veins, moreover, a redox agent like CH_4 or H_2S is required that is probable related to a third endmember 3 as endmember 1 and 2 are likely both too oxidized for the related low oxygen fugacities (probably hydrocarbon in the Nama basin (Walter et al., 2023), see also analogue studies: Walter et al., 2018a, 2018b; Walter et al., 2019). As known from European analogue studies, it is assumed that the metal content in the mixed fluid negatively correlates with Ca (provided by the Nama Group limestone derived fluid), which would indicate that most metals are carried by the endmember 1 brine that reacted with the primary minerals of the Namaqua-Natal-Metamorphic province gneisses (Walter et al., 2023). During the desiccation process and related clay mineral formation in the crystalline basement, metals were released into the fluid at contemptuously water consumption which lead to an increasing residual salinity (Burisch et al., 2016; Walter et al., 2019, 2023). However, the process of primary vein formation does not explain the pseudmorphic and perimorphic replacements that characterize the hydrothermal veins at Weltevrede and Mickberg. To generate such textures additional processes, which were not observable at Garub farm and Aukam valley (Walter et al., 2023, c), are needed.

4.2. *Processes leading to the pseudomorphous and perimorphous replacements*

To understand the pseudomorphous replacement of baryte by siderite in the Mesozoic hydrothermal system of southern Namibia, it is crucial to constrain the formation conditions and to decipher the general processes that can lead to baryte dissolution and siderite precipitation in hydrothermal settings.

Baryte dissolution: Baryte commonly precipitates by fluid mixing of a sulfate and a barium bearing fluid (Walter et al., 2018a, 2019; 2023a, 2023b). Baryte solubility at hydrothermal conditions is generally dependent on [1] temperature (both, an appropriate decrease or increase in temperature may cause baryte dissolution; Blount, 1977; Monnin, 1999), [2] pressure (an increase in pressure can initiate baryte dissolution; (Blount, 1977; Monnin, 1999), [3] fluid composition (a decrease in either barium or sulfate content of the fluid may increase baryte dissolution; (Shi et al., 2012)), and [4] redox condition of the involved fluid. Furthermore, a change in ionic strength of the

hydrothermal fluid also affects the solubility of baryte. In respect to the conditions predominating the formation of hydrothermal veins at Weltevrede and Mickberg a change in baryte solubility due to temperature changes is typically small (at a trapping temperature of about 150 °C in average) and strongly dependents on salinity and pressure (Blount, 1977). Hence, a change in temperature is unlikely the reason for baryte dissolution on a scale present at Weltevrede and Mickberg. A pressure increase is also unlikely as no evidence is given to assume changing pressure condition at the formation depth (Namaqua-Natal-Metamorphic Complex /Nama Group unconformity at about 1 km below paleosurface) of the hydrothermal veins. Additionally, no evidence for brecciation can be observed which would support a pressure increase. Thus, it is most likely that pre-existing baryte was dissolved by a late stage fluid with a composition that differs from the baryte generating fluid and is undersaturated in baryte (low sulfur and/or barium content). This dissolution process can also be promoted by the presence of abundant complex forming ligands. Most important for the fluid in question is Cl and carbonate (this study, Walter et al., 2023a; 2023b). At high carbonate contents the formation of Ba-carbonate complexes, such as $Ba(HCO_3)^+$ (Apps and Wilkin, 2015; Nordstrom et al., 1990), greatly increases the solubility of baryte at neutral to alkaline and oxidizing conditions (Fig. 8b).

The dissolution of baryte is strongly dependent on the redox state of the involved fluid. At conditions above the sulfate/sulfide boundary, a fluid at roughly neutral condition dissolves baryte by the following reaction:

$$\text{baryte} \rightarrow SO_4^{2-} + Ba^{2+} \quad (1)$$

At more reducing equilibrium conditions, baryte dissolves through the redox reactions of:

$$\text{baryte} + H^+ \rightarrow Ba^{2+} + HS^- + 2\,O_2(aq)\ (\text{at } 150^\circ C > 6.5pH) \quad (2)$$

$$\text{baryte} + 2H^+ \rightarrow Ba^{2+} + H_2S(aq) + 2\,O_2(aq)\ (\text{at } 150^\circ C < 6.5pH) \quad (3)$$

When discussing redox reactions of sulfur species, the sluggish kinetics of reactions between sulfides and sulfates at abiotic environments with temperatures below ~300 °C, which strongly depend on the type of reducing/oxidizing agent and the fluid pH (Ohmoto and Lasaga, 1982) have to be considered. This sluggishness plays a crucial role in the formation or absence of thermodynamically stable minerals in other hydrothermal assemblages (Scharrer et al., 2019). However, the formation

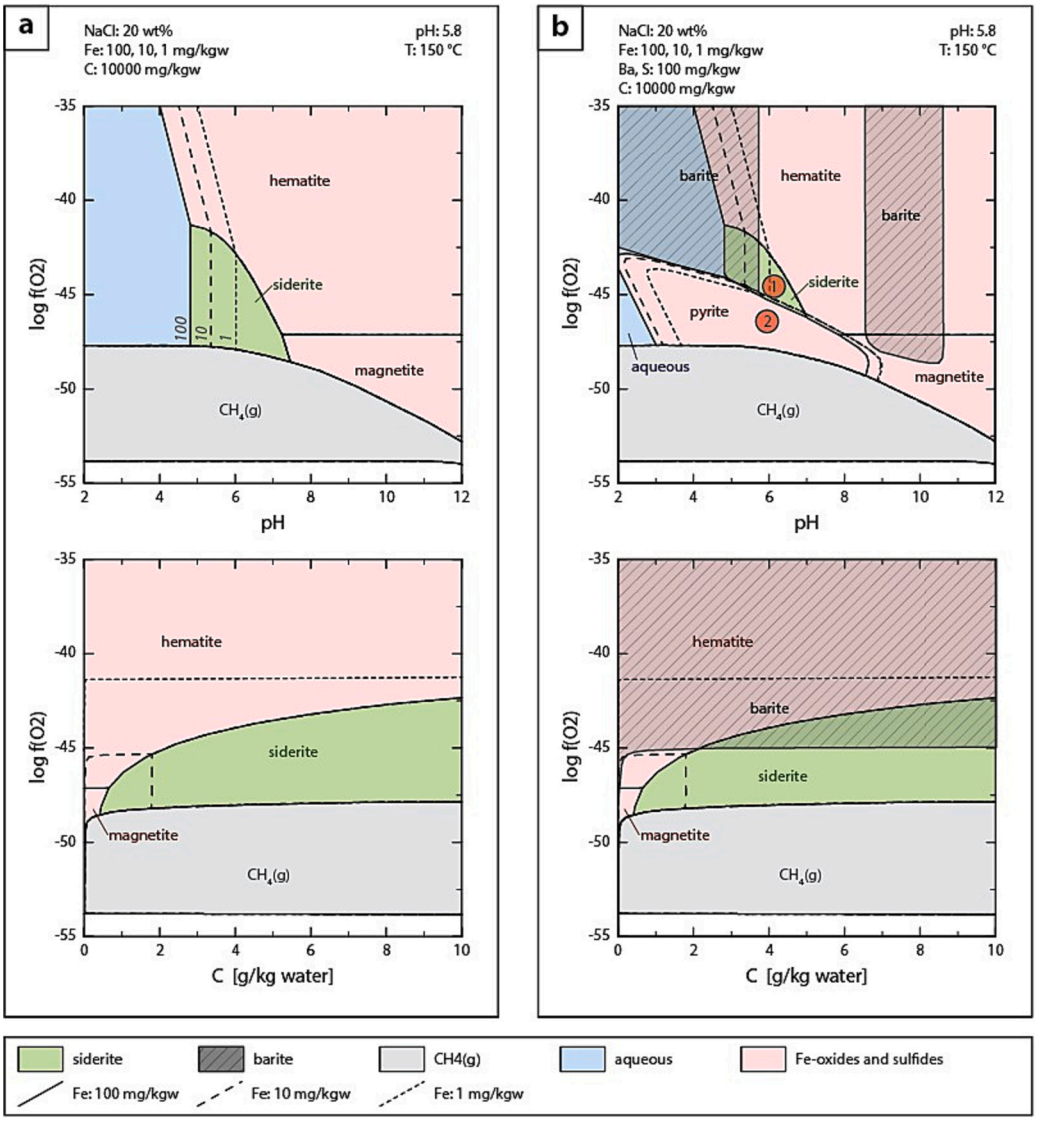

Fig. 8. *Thermodynamic predominance stability model at 150 °C using typical compositional ranges of fluids in the region. Neutral pH at 150 °C is approximately 5.8.* (A) Simplified Fe-C-Na-Cl-H-O system with respect to fO_2, pH **(upper diagram)** and C-content **(lower diagram)**. (B) More complex Fe-C-Ba-S-Na-Cl-H-O system with respect to fO_2, pH **(upper diagram)** and C-content **(lower diagram)**.

of pseudormorphous siderite after baryte is likely to be kinetically controlled as well. Reducing conditions promote the baryte dissolution while simultaneously siderite precipitation is supported. Partial replacement textures indicate not fully complete dissolution and precipitation reactions, i.e. no global equilibrium reached, which further underlines the importance of the temporal aspect due to kinetics. Unfortunately, experimental kinetic data to confirm this is lacking so far.

Siderite precipitation: Thermodynamic modelling reveals that the formation of siderite is constrained to a redox state that approximately matches the hematite-magnetite buffer and a roughly neutral pH (4.5–8; Fig. 8a). In this environment, siderite precipitation can occur due to [1] a temperature increase, [2] an increase in pH, [3] an increase in Fe or [4] an increase in f_{CO2} (Fig. 8). In the temperature range of 100 to 200 °C an increase of about 50 °C would change the solubility constant of siderite by one order of magnitude in favour of precipitation (Bénézeth et al., 2009). Although a temperature increase of about 50 °C would be generally possible for the investigated location, direct evidence is lacking. Moreover, an increase in fluid temperature would also be associated with a, at least partial, dissolution of quartz (Akinfiev and Diamond, 2009). There is, however, no evidence for quartz dissolution in any samples. A low Ca/Fe ratio of the fluid is also crucial ($\sim < 150$), to avoid calcite precipitation instead of siderite. Thus, by elimination of unlikely processes/conditions a change in fluid chemistry combined with reducing conditions is most likely responsible for siderite formation.

Siderite pseudomorph after baryte: The direct reaction textures of siderite pseudomorphs after baryte as well as the lack of abundant vacant baryte crystals perimorphosed by quartz supports the conclusion that the precipitation of siderite is directly (temporarily and spatially) linked to the dissolution of baryte. These findings rule out the possibility of two distinct processes that independently caused baryte dissolution and siderite precipitation. However, a redox state above the sulfate-sulfide boundary, a dissolution of baryte (reaction 1) does not influence the solubility of siderite. Thus, an independent mechanism must be involved in the formation of siderite pseudomorphs that formed under such higher oxidizing conditions, to enable a simultaneously baryte dissolution and siderite precipitation. In contrast, under more reducing conditions (below the sulfate-sulfide boundary), the dissolution of baryte and reduction of the sulfate to sulfide (sulfate-sulfide redox reactions) directly force the fluids to a more basic pH (reactions 2 & 3) as H^+ is attached to sulfur. This greatly decreases the solubility of siderite and thus siderite can oversaturate. In this case, precipitation of siderite would occur by one of the following reactions, depending on pH:

$$HCO_3^- + Fe^{2+} \rightarrow \text{siderite} + H^+ \ (\text{at } 150^\circ\text{C} > 6.7\text{pH}) \quad (4)$$

$$CO_{2(aq)} + Fe^{2+} + H_2O \rightarrow \text{siderite} + 2H^+ \ (\text{at } 150^\circ\text{C} < 6.7\text{pH}) \quad (5)$$

Under these conditions, hydrogensulfide species will form (see reactions 2 & 3). Dissolved Fe (presence of this is given due the formation of abundant siderite), shows a low solubility in the presence of hydrogensulfide. Thermodynamic modelling shows that this would lead to the formation of pyrite until the aqueous sulfide species have been consumed.

$$2HS^- + Fe^{2+} \rightarrow \text{pyrite} + 2\,H^+ \ (\text{at } 150^\circ\text{C} > \sim 6.5\text{pH}) \quad (6)$$

$$2\,H_2S(aq) + Fe^{2+} \rightarrow \text{pyrite} + 4H^+ \ (\text{at } 150^\circ\text{C} > \sim 6.5\text{pH}) \quad (7)$$

Under these conditions pyrite precipitation releases H^+ ions. That, in turn, enhance the dissolution of baryte by sulfate reduction. In the hydrothermal veins at Weltevrede and Mickberg, up to centimetre large pyrite crystals are directly associated with the siderite pseudomorphs. Thus, both thermochemical and textural evidence indicates that pyrite formation is a side effect of baryte dissolution under reduced conditions.

5. Conclusion

In conclusion, the mineral association in addition to thermodynamic modelling of a well defined hydrothermal fluid system from the literature enables the investigation of how siderite pseudomorphs after baryte form. Their formation is constrained to reducing conditions, under which sulfate is reduced and the dissolution of baryte promotes siderite and pyrite precipitation. Studies like the one presented here, are substantial to shed light on post-ore stage modifications in hydrothermal systems that can have significant influence of the ore grade and tonnages of metal ores and industrial minerals like baryte. One of the most important results is the role of fluid cooling, which is suggested as a crucial component in a regional scale fluid system to trigger post-precipitation mineralogical modifications by pseudomorphic and perimorphic replacements. Nevertheless, the present study only targets one single process of pseudomorphic replacement. Since silification and sideritization can significantly influence the economic potential of a deposit, more research is needed to address the various types of replacement systematically.

CRediT authorship contribution statement

Benjamin F. Walter: Writing – review & editing, Writing – original draft, Visualization, Validation, Supervision, Resources, Project administration, Methodology, Investigation, Funding acquisition, Formal analysis, Data curation, Conceptualization. **Manuel Scharrer:** Writing – review & editing, Writing – original draft, Visualization, Methodology, Investigation, Formal analysis, Data curation, Conceptualization. **R. Johannes Giebel:** Writing – review & editing, Writing – original draft, Visualization, Methodology, Investigation, Conceptualization. **Aratz Beranoaguirre:** Methodology, Investigation. **Jorge C.L. Arthuzzi:** Writing – original draft, Investigation. **Lorenz Kemmler:** Writing – review & editing, Writing – original draft, Investigation. **Andreja Ladisic:** Writing – review & editing, Writing – original draft, Visualization, Methodology, Investigation, Data curation. **Saskia Dück:** Writing – review & editing, Writing – original draft, Visualization, Data curation, Conceptualization. **Michael Marks:** Writing – review & editing, Writing – original draft, Project administration, Funding acquisition, Conceptualization. **Gregor Markl:** Writing – review & editing, Writing – original draft, Supervision.

Declaration of competing interest

The authors declare the following financial interests/personal relationships which may be considered as potential competing interests: Benjamin Walter reports financial support was provided by German Research Foundation. Johannes Giebel reports financial support was provided by German Research Foundation. Michael Marks reports financial support was provided by German Research Foundation. If there are other authors, they declare that they have no known competing financial interests or personal relationships that could have appeared to influence the work reported in this paper.

Acknowledgments

We thankful acknowledge two annoymous reviewer for their critical reviews and Martina Zucchi and Astrid Holzheid for editorial guidance. Elisabeth Eiche und Maja Denker are thankfully acknowledged for their help with crush leach analyses. This work has not received funding but the samples were gathered during fieldwork related to the DFG project Magma evolution in space and time along the Kuboos Bremen Line in Namibia (grant WA3116/14–1, GI1499/5–1, MA2563/25–1). Moreover, the LA-ICPMS facility at LERA KIT is supported by DFG grant INST 121384/213–1 FUGG.

Appendix A. Supplementary data

Supplementary data to this article can be found online at https://doi.org/10.1016/j.chemer.2024.126244.

References

Akinfiev, N.N., Diamond, L.W., 2009. A simple predictive model of quartz solubility in water–salt–CO2 systems at temperatures up to 1000°C and pressures up to 1000 MPa. Geochim. Cosmochim. Acta 73 (6), 1597–1608.

Apps, J.A., & Wilkin, R.T., (2015). Thermodynamic Properties of Aqueous Carbonate Species and Solid Carbonate Phases of Selected Trace Elements Pertinent to Drinking Water Standards of the US Environmental Protection Agency Report. Lawrence Berkeley (National Lab (LBNL), Berkeley, CA (United States).

Baier, E., Venzlaff, V., Bodenforsch, L.A., 1961. Über die Verquarzung von Barytgängen. Notizblatt des Hessischen Landesamtes für Bodenforschung zu Wiesbaden 89, 365–376.

Baumann, L., Kuschka, E., Seifert, T., 2000. Lagerstätten des Erzgebirges. Enke im (Thieme-Verlag). 300p.

Bénézeth, P., Dandurand, J., Harrichoury, J., 2009. Solubility product of siderite (FeCO3) as a function of temperature (25–250°C). Chem. Geol. 265 (1–2), 3–12.

Blanc, P., 2017. Update for the 2017 version. In report BRGM/RP-66811-FR. http://thermoddem.brgm.fr/.

Blanc, P., Lassin, A., Piantone, P., Azaroual, M., Jacquemet, N., Fabbri, A., Gaucher, E.C., 2012. Thermoddem: a geochemical database focused on low temperature water/rock interactions and waste materials. Appl. Geochem. 27 (10), 2107–2116.

Bliedtner, M., Martin, M., 1986. Erz-und Minerallagerstatten des Mittleren Schwarzwaldes: eine bergbauge-schichtliche und lagerstattenkundliche Darstellung. Geologisches Landesamt Baden-Württemberg, Germany.

Blount, C., 1977. Baryte solubilities and thermodynamic quantities up to 300°C and 1400 bars. Am. Mineral. 62 (9–10), 942–957.

Burisch, M., Markl, G., Gutzmer, J., 2022. Breakup with benefits-hydrothermal mineral systems related to the disintegration of a supercontinent. Earth Planet. Sci. Lett. 580, 117373.

Burisch, M., Walter, B.F., Markl, G., 2017. Silicification of hydrothermal gangue minerals in Pb-Zn-cu-fluorite-quartz-baryte veins. Can. Mineral. 55 (3), 501–514.

Burisch, M., Walter, B.F., Wälle, M., Markl, G., 2016. Tracing fluid migration pathways in the root zone below unconformity-related hydrothermal veins: insights from trace element systematics of individual fluid inclusions. Chem. Geol. 429, 44–50.

Corner, B., 2000. Crustal framework of Namibia derived from magnetic and gravity data. Communications of the Geological Survey of Namibia 12, 13–19.

Davisson, M.L, & Criss, R.E., (1996). Na-ca-Cl relations in basinal fluids. Geochim. Cosmochim. Acta, 60, 2743–2752.

Dong, G., Morrison, G., Jaireth, S., 1995. Quartz textures in epithermal veins, Queensland; classification, origin and implication. Econ. Geol. 90 (6), 1841–1856.

Epp, T., Walter, B.F., Scharrer, M., Lehmann, G., Henze, K., Heimgärtner, C., Bach, W., Markl, G., 2019. Quartz veins with associated Sb-Pb-ag±au mineralization in the Schwarzwald, SW Germany: a record of metamorphic cooling, tectonic rifting, and element remobilization processes in the Variscan belt. Mineral. Deposita 54, 281–306.

Goldstein, R.H., & Reynolds, T.J., (1994). Systematics of Fluid Inclusions in Diagenetic Minerals. Short Course 31, Society of Economic Paleontologists and Mineralogists, Tulsa. 199 p.

Grotzinger, J., Adams, E.W., Schroder, S., 2005. Microbial–metazoan reefs of the terminal Proterozoic Nama group (c. 550–543 ma). Namibia. Geological Magazine 142 (5), 499–517.

Hoal, B.G., 1990. The geology and geochemistry of the Proterozoic Awasib Mountain terrain, southern Namibia. Memorandum of the Geological Survey of Namibia 11, 163.

Jochum, K.P., Weis, U., Stoll, B., Kuzmin, D., Yang, Q., Raczek, I., Jacob, D.E., Stracke, A., Birbaum, K., Frick, D.A., Günther, D., 2011. Determination of reference values for NIST SRM 610–617 glasses following ISO guidelines. Geostand. Geoanal. Res. 35 (4), 397–429.

Kinniburgh, D., Cooper, D., 2011. PhreePlot: Creating Graphical Output with PHREEQC. Software User Manual.

Kolchugin, A., Immenhauser, A., Morozov, V., Walter, B., Eskin, A., Korolev, E., Neuser, R., 2020. A comparative study of two Mississippian dolostone reservoirs in the Volga-Ural Basin. Russia. *Journal of Asian Earth Sciences* 199, 104465.

Kolchugin, A.N., Immenhauser, A., Walter, B.F., Morozov, V.P., 2016. Diagenesis of the palaeo-oil-water transition zone in a lower Pennsylvanian carbonate reservoir: constraints from cathodoluminescence microscopy, microthermometry, and isotope geochemistry. Mar. Pet. Geol. 72, 45–61.

Kreissl, S., Gerdes, A., Walter, B.F., Neumann, U., Wenzel, T., Markl, G., 2018. Reconstruction of a > 200 ma multi-stage "five element" bi-co-Ni-Fe-as-S system in the Penninic Alps, Switzerland. Ore Geol. Rev. 95, 746–788.

Leach, D.L., Marsh, E., Emsbo, P., Rombach, C.S., Kelley, K.D., Anthony, M., 2004. Nature of hydrothermal fluids at the shale-hosted red dog Zn-Pb-ag deposits, Brooks Range. Alaska. Economic Geology 99 (7), 1449–1480.

Liessmann, D.-M.D.W., (2010). Kupfer, Eisen und Schwerspat–Die Schatze des Sudwestharzes. *Historischer Bergbau im Harz. Springer*, Berlin, Germany, 259–284.

Lindgren, W., 1899. Veins of Silver City and De Lamar, Idaho. *United States geological survey, 20th.* Annu. Rep. 3, 107–188.

Macey, P.H., Thomas, R.J., Kisters, A.F.M., Diener, J.F.A., Angombe, M., Doggart, S., Groenewald, C.A., Lambert, C.W., Miller, J.A., Minnaar, H., Smith, H., 2022. A continental back-arc setting for the Namaqua belt: evidence from the Kakamas domain. Geosci. Front. 13 (4), 101408.

Monnin, C., 1999. A thermodynamic model for the solubility of baryte and celestite in electrolyte solutions and seawater to 200°C and to 1 kbar. Chem. Geol. 153 (1–4), 187–209.

Morgan, P.G., (1925). The so-called" pseudomorphous" quartz of tertiary gold-silver veins. Econ. Geol., 20, 203–207.

Müller, M., Walter, B.F., Giebel, R.J., Beranoaguirre, A., Swart, P.K., Lu, C., Riechelmann, S., Immenhauser, A., 2024. Towards a better understanding of the geochemical proxy record of complex carbonate archives. Geochimica et cosmochimica acta.

Mueller, M., Igbokwe, O.A., Walter, B., Pederson, C.L., Riechelmann, S., Richter, D.K., Albert, R., Gerdes, A., Buhl, D., Neuser, R.D., Bertotti, G., 2020. Testing the preservation potential of early diagenetic dolomites as geochemical archives. Sedimentology 67 (2), 849–881.

Mueller, M., Jacquemyn, C., Walter, B.F., Pederson, C.L., Schurr, S.L., Igbokwe, O.A., Jöns, N., Richelmann, S., Dietzel, M., Strauss, H., Immenhauser, A., 2022a. Constraints on the preservation of proxy data in carbonate archives–lessons from a marine limestone to marble transect, Latemar. Italy. *Sedimentology* 69 (2), 423–460.

Mueller, M., Walter, B.F., Swart, P.K., Jöns, N., Jacquemyn, C., Igbokwe, O.A., Immenhauser, A., 2022b. A tale of three fluids: fluid-inclusion and carbonate clumped-isotope paleothermometry reveals complex dolomitization and dedolomitization history of the Latemar platform. J. Sediment. Res. 92 (12), 1141–1168.

Nordstrom, D.K., Plummer, L.N., Langmuir, D., Busenberg, E., May, H.M., Jones, B.F., Parkhurst, D.L., 1990. Revised chemical equilibrium data for major water—mineral reactions and their limitations. ACS 416 (Publications).

Ohmoto, H., Lasaga, A.C., 1982. Kinetics of reactions between aqueous sulfates and sulfides in hydrothermal systems. Geochim. Cosmochim. Acta 46 (10), 1727–1745.

Parkhurst, D.L., 1995. User's Guide to PHREEQC: A Computer Program for Speciation, Reaction-Path, Advective-Transport, and Inverse Geochemical Calculations. US Department of the Interior, US Geological Survey.

Parkhurst, D.L., Appelo, C., 1999. User's guide to PHREEQC (version 2): a computer program for speciation, batch-reaction, one-dimensional transport, and inverse geochemical calculations. Water-resources investigations report 99 (4259), 312.

Paton, C., Hellstrom, J., Paul, B., Woodhead, J., Hergt, J., 2011. Iolite: freeware for the visualisation and processing of mass spectrometric data. J. Anal. At. Spectrom. 26 (12), 2508–2518.

Pearce, N.J., Perkins, W.T., Westgate, J.A., Gorton, M.P., Jackson, S.E., Neal, C.R., Chenery, S.P., 1997. A compilation of new and published major and trace element data for NIST SRM 610 and NIST SRM 612 glass reference materials. Geostand. Newslett. 21 (1), 115–144.

Reid, D.L., Cooper, A.F., Rex, D.C., Harmer, R.E., 1990. Timing of post–Karoo alkaline volcanism in southern Namibia. Geol. Mag. 127 (5), 427–433.

Sandberger, F., 1891. Ueber dieErzgange der Gegend von Freudenstadt und Bulach im württembergischen Schwarzwald, vol. 21. Sitzungsberichte der Mathematisch-Physikalischen Classe der Königlich Bayerischen Akademie der Wissenschaften, pp. 281–318.

Scharrer, M., Kreissl, S., Markl, G., 2019. The mineralogical variability of hydrothermal native element-arsenide (five-element) mineralizations and the role of aqueous sulfide. Ore Geol. Rev. 113, 103025.

Schrader, F.S., 1912. A reconnaissance of the Jarbidge, contact and elk mountain mining districs, Elko country, Silicification of hydrothermal gangue minerals in Pb-Zn-cu veins 13 Nevada. United States Geological Survey Bulletin 497, 162p.

Shi, W., Kan, A.T., Fan, C., Tomson, M.B., 2012. Solubility of Baryte up to 250°C and 1500 bar in up to 6 m NaCl solution. Ind. Eng. Chem. Res. 51 (7), 3119–3128.

Steele-MacInnis, M., Bodnar, R.J., Naden, J., 2011. Numerical model to determine the composition of H2O–NaCl–CaCl2 fluid inclusions based on microthermometric and microanalytical data. Geochim. Cosmochim. Acta 75 (1), 21–40.

Steele-MacInnis, M., Lecumberri-Sanchez, P., Bodnar, R.J., 2012. HokieFlincs_H2O-NaCl: a Microsoft excel spreadsheet for interpreting microthermometric data from fluid inclusions based on the PVTX properties of H2O–NaCl. Comput. Geosci. 49, 334–337.

Verwoerd, W.J., 1967. The carbonatites of South Africa and south West Africa. Handbook of the Geological Survey of South Africa. 6, 452.

Walter, B.F., Burisch, M., Fusswinkel, T., Marks, M.A.W., Steele-MacInnis, M., Wälle, M., Apukhtina, O., Markl, G., 2018a. Multi-reservoir fluid mixing processes in rift-related hydrothermal veins, Schwarzwald, SW-Germany. J. Geochem. Explor. 186, 158–186.

Walter, B.F., Gerdes, A., Kleinhanns, I.C., Dunkl, I., von Eynatten, H., Kreissl, S., Markl, G., 2018b. The connection between hydrothermal fluids, mineralization, tectonics and magmatism in a continental rift setting: fluorite Sm-Nd and hematite and carbonates U-Pb geochronology from the Rhinegraben in SW Germany. Geochim. Cosmochim. Acta 240, 11–42.

Walter, B.F., Giebel, J., Marlow, A.G., Siegfried, P.R., Marks, M., Markl, G., Palmer, M., Kolb, J., 2022. The Kieshöhe carbonatites of southwestern Namibia–the post-magmatic role of silicate xenoliths on REE mobilisation. Communications of the Geological Survey of Namibia 25, 1–31.

Walter, B.F., Giebel, R.J., Siegfried, P., Doggart, S., Macey, P., Schiebel, D., Kolb, J., 2023. The genesis of hydrothermal veins in the Aukam valley SW Namibia–a far field consequence of Pangean rifting? J. Geochem. Explor. 250, 107229.

Walter, B.F., Immenhauser, A., Geske, A., Markl, G., 2015. Exploration of hydrothermal carbonate magnesium isotope signatures as tracers for continental fluid aquifers, Schwarzwald mining district, SW Germany. Chem. Geol. 400, 87–105.

Walter, B.F., Kortenbruck, P., Scharrer, M., Zeitvogel, C., Wälle, M., Mertz-Kraus, R., Markl, G., 2019. Chemical evolution of ore-forming brines–basement leaching, metal

provenance, and the redox link between barren and ore-bearing hydrothermal veins. A case study from the Schwarzwald mining district in SW-Germany. Chem. Geol. 506, 126–148.
Walter, B.F., Giebel, R.J., Arthuzzi, J.C., Kemmler, L., Kolb, J., 2024. Diatreme-hosted fluorite mineralization in S-Namibia–A tale of cryogenic brine formation and fluid mixing below an unconformity in the context of Pangea rifting. J. Afr. Earth Sci. 210, 105154.
Wark, D.A., Watson, E.B., 2006. TitaniQ: a titanium-in-quartz geothermometer. Contrib. Mineral. Petrol. 152 (6), 743–754.